OXIDATIVE-REFORMING OF METHANE AND PARTIAL OXIDATION OF METHANE REACTIONS OVER NiO/PrO$_2$/ZrO$_2$ CATALYSTS: EFFECT OF NICKEL CONTENT

Y. J. O. Asencios[1], F. C. F. Marcos[2], J. M. Assaf[3] and E. M. Assaf[2*]

[1]Instituto do Mar, Universidade Federal de São Paulo, CEP: 11070-100, Santos - SP, Brazil.
E-mail: yvan.jesus@unifesp.br
[2]Instituto de Química de São Carlos, Universidade de São Paulo, CEP: 13560-970, São Carlos - SP, Brazil.
*E-mail: eassaf@iqsc.usp.br
[3]Departamento de Engenharia Química, Universidade Federal de São Carlos,
CEP: 13565-905, São Carlos - SP, Brazil.

Abstract - In this work the behavior of NiO-PrO$_2$-ZrO$_2$ catalysts containing various nickel loadings was evaluated in the partial oxidation of methane and oxidative-reforming reactions of methane. The catalysts were characterized by X-Ray Diffraction Analysis (*in situ*-XRD), Temperature Programmed Reduction (H$_2$-TPR), Scanning Electron Microscopy (SEM/EDX) and Adsorption-Desorption of nitrogen (BET area). The reactions were carried out at 750 °C and 1 atm for 5 hours. The catalysts were studied with different nickel content: 0, 5, 10 and 15% (related to total weight of catalyst, wt%). In both reactions, the catalyst containing the mixture of the three oxides (NiO/PrO$_2$/ZrO$_2$) with 15% nickel (15NiPrZr catalyst) showed the best activity for the conversion of the reactants into Syngas and showed high selectivity for H$_2$ and CO. The results suggest that the promoter PrO$_2$ and the Ni^o centers are in a good proportion in the catalyst with 15% Ni. Our results showed that low nickel concentrations in the catalyst led to high metallic dispersion; however, very low nickel concentrations did not favor the methane transformation into Syngas. The catalyst containing only NiO/ZrO$_2$ in the mixture was not sufficient for the catalysis. The presence of the promoter PrO$_2$ was very important for the catalysis of the POM.
Keywords: Reforming methane; Partial-oxidation; Syngas; Nickel-content; Praseodymium.

INTRODUCTION

Methane is a light hydrocarbon found mainly in natural gas, biogas and shale gas. Methane can also be obtained from the pyrolysis of biomass (in the absence of oxygen); the principal gaseous products coming from this process are CO, CO$_2$, CH$_4$, H$_2$ and N$_2$ (Couto *et al.*, 2013; Turn *et al.*, 1998). Methane is the major composition of so-called Shale gas (carbon dioxide, ethane and propane are present to a lesser extent), which is the natural gas found trapped within porous sedimentary Shale rock (Wright *et al.*, 2015). Shale gas can be used directly as a fuel to generate electricity; however, this use has generated much discussion and controversy, since it emits more greenhouse gases than electricity generated from natural gas or coal (Burnham *et al.*, 2012).

On the other hand, the use of methane directly as fuel would not be completely advantageous because it generates carbon dioxide, which contributes to the greenhouse effect. Furthermore, the transportation of methane from the source reservoir to the place where

it will be used can be dangerous and expensive (Asencios *et al*., 2012a). Thus, the transformation of this methane through the reforming reactions to generate a high valued product such as Synthesis Gas (Syngas, a mixture of H_2 and CO) is an attractive alternative way to use methane efficiently. Syngas may be used to generate electricity, as a fuel in some types of engines, or may also be transformed into a complex array of products such as: alkanes, paraffin and oxygenates (as aldehydes and ketones) by the Fischer-Tropsch synthesis (Ramos *et al*., 2011). The current technology, named the Gas-to-Liquid process (GTL process), consists of the Fischer-Tropsch Synthesis as the principal process. These products have advantages from various points of view: environmental, economic and logistic (Cheng *et al*., 2015).

Since it is known that the major components of biogas are methane and carbon dioxide, the biogas (free of impurities such as NH_3, H_2S, among other trace products) can be transformed directly by the dry reforming of methane (DRM, Reaction 1) into syngas (Sun *et al*., 2010; Rueangjitt *et al*., 2012):

$$DRM: \ CH_4 + CO_2 \rightarrow 2CO + 2H_2$$

$$\Delta H°_{298} = \ 247 \ (kJ/mol) \tag{1}$$
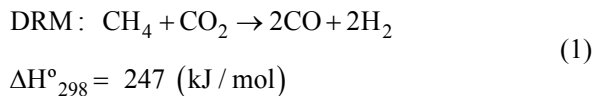
The partial oxidation of methane (POM, Reaction 2), owing to its exothermic nature, is a rapid reaction, and generates energy to maintain the reaction for long-term operations and the presence of O_2 reduces the coke deposit by increasing the lifetime of the catalyst:

$$POM: \ 2CH_4 + O_2 \rightarrow 2 \ CO + 4 \ H_2$$

$$\Delta H° = -22.6 \ kJ.mol^{-1} \tag{2}$$
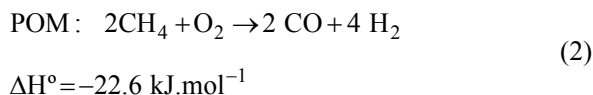
However, one main disadvantage of POM is that it requires pure oxygen; furthermore, the exothermicity of POM leads to hot spots on the catalyst, which cause problems for the reactor, making the process hazardous and hard to control. An interesting process would be to combine POM with DRM (an endothermic reaction) in the Oxidative Reforming of Methane (ORM) (Asencios *et al*., 2012b):

$$ORM: \ 1.5CH_4 + CO_2 + 0.25 \ O_2 \rightarrow 2.5CO + 3H_2 \tag{3}$$

$$\Delta H° = 249.2 kJ.mol^{-1}$$
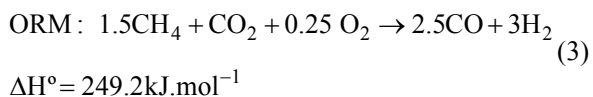
The ORM could be carried out in an adiabatic reactor without heat supply, thus reducing the formation of hot spots and making the process energy

efficient. Furthermore, by manipulating the molar relation of reactants in the ORM, the H_2/CO ratio could be controlled for various synthetic purposes (Lucrédio *et al*., 2012; Olah *et al*., 2013).

The most active catalysts for methane reforming reactions are the noble metals-based catalysts (such as Pt, Pd, Rh, Ru). The non-noble metal-based catalysts, such as Ni and Co, present activity as well; however, they present problems due to carbon formation, which is undesirable because it leads to catalyst deactivation and increases the reactor pressure, which may lead to explosion. At this point, it is relevant to mention that Brazil occupies an important position in world nickel production (Mood, 2010).

In our previous papers we found that nickel supported on solid-solutions composed of MgO/ZrO_2 (Asencios *et al*., 2011; Asencios *et al*., 2012a; Asencios *et al*., 2012b) or Y_2O_3/ZrO_2 (Asencios *et al*. 2013) resulted in good catalysts (stable performance and coke-resistant) for ORM and POM reactions. On the other hand, the properties of PrO_2 such as oxygen storage capacity, oxygen vacancies and redox (owing to the oxidation states Pr^{3+}/Pr^{4+}) are well known and documented (Liu *et al*., 2011). Pr has been used as a promoter of Ni based catalysts for various reforming reactions, as described by Gallego *et al*. 2009) for perovskite (Ni/La/O) derived catalysts; by Gamba *et al*. (2011) for Ni catalysts supported on smectite, and by Barroso *et al*. (2011) for Ni catalysts supported on $MgAl_2O_4$. It is assumed that the promoter properties of Pr are based on the generation of superficial oxygen vacancies, which favor the neighborhood of the metallic phase in the supported catalyst and assist the removal of coke deposits. In view of the referred studies, in the present paper we explore the catalytic performance of nickel supported on PrO_2/ZrO_2, with various nickel loadings, aiming to find the optimal nickel content in this system to the reach the maximum catalytic performance in the ORM and POM reactions to produce Syngas from methane from different sources.

EXPERIMENTAL

Preparation of Catalysts

The catalytic supports were prepared by the Pechini polymerization method (Marcos and Gouvêa, 2004), using $Zr(CO_3)_2.1.5H_2O$, citric acid ($C_6H_8O_7$) and ethylene glycol ($C_2H_6O_2$). The zirconium carbonate was dissolved in nitric acid and then added to an aqueous solution of citric acid and ethylene glycol (mass ratio of 60 citric acid: 40 ethylene glycol); the

polymer was formed by heating this mixture to 120 °C and keeping it at this condition for 24h. The obtained polymer was dried at 90 °C for 12 h and then calcined at 750 °C (5 °C.min⁻¹) in synthetic air (21%O₂/79%N₂) for 2 h. The resulting material was the catalytic support.

The nickel and praseodimium were added in the form of nitrates: $Ni(NO_3)_3.6H_2O$ and $Pr(NO_3)_3.6H_2O$, by the impregnation method in the catalytic support. For this procedure, the nickel and praseodimium salts were dissolved in distilled water and then added to the catalytic support (prepared by the above procedure, ZrO_2), forming a suspension. This mixture was maintained at 80 °C under reduced pressure to completely remove the solvent (using a rotary evaporator); after this step, the mixture was dried at 100 °C (12 h) and then calcined at 750 °C (5 °C.min⁻¹) for 3 h, under synthetic air flow (30 mL.min⁻¹) to obtain the oxide phases. The mass relation of PrO_2/ZrO_2 was kept constant at 1%; and the nickel content was varied as follows: 0, 5, 10 and 15 wt% relative to total catalyst; the catalysts were designated PrZr, 5NiPrZr, 10NiPrZr, and 15NiPrZr, respectively. For the purpose of comparison, a sample containing 15 wt% of Ni supported on ZrO_2 (the support synthesized by the Pechini method) was prepared by the impregnation method (sample 15NiZr) and then heat-treated under the same conditions as the other catalysts; this sample represents the catalyst without the praseodimiun promoter.

Characterization

The crystal phases were studied by the *in situ* X-ray diffraction technique, which was conducted with a 6-circle diffractometer (Huber) at the beamline D10B-XPD of the Brazilian Synchrotron Light Laboratory (LNLS) in Campinas, Brazil. The X-ray wavelength used was 1.5406 Å and the Bragg angle was scanned continuously in the range 2Θ = 20-70° at an angular speed of 0.02° s⁻¹. Approximately 50 mg of the powder sample was placed in a ceramic sample holder. The XRD pattern was acquired under ambient conditions (25 °C and synthetic air) and under reduction conditions. For this last condition, the catalyst was heated in a 50 mL min⁻¹ H₂ stream (5% H₂/He) from room temperature to 650 °C, at a rate of 5 °C.min⁻¹. The XRD pattern was collected *in situ* at 700 °C for each catalyst.

The specific surface area (BET) was estimated from the N₂ adsorption/desorption isotherms at liquid nitrogen temperature, using a Quantachrome Nova 1200 instrument. Temperature-programmed reduction (TPR) was performed in a quartz tube reactor and hydrogen consumption was measured with a thermal conductivity detector (TCD). For this analysis, 100 mg of catalyst was placed in the TPR reactor and reduced with a 5% H₂–95% He (v/v) gas mixture flowing at 30 mL.min⁻¹; the temperature was increased to 1000 °C at a heating rate of 5 °C.min⁻¹.

Scanning electron microcopy (SEM) images of spent catalysts were taken in a LEO 440 microscope with an Oxford detector, operating with a 20 kV electron beam. The samples were made up in the form of pellets and coated with a layer of gold to avoid a charge build-up. The composition of the catalysts was determined by energy-dispersive X-ray spectroscopy (EDX); the measurements were made in five regions of the image using a LEO 440 scanning electron microscope with a tungsten filament coupled to an energy-dispersive X-ray detector.

The spent catalysts were analyzed by Thermogravimetric Analyses (TG) with a SDT2960 Instrument to explore the carbon deposits formed during the POM reaction. Samples were heated at 10 °C min⁻¹, from room temperature to 1000 °C, with an air flow of 100 mL.min⁻¹.

Catalytic Test

Catalytic reactions were carried out with 100 mg of catalyst in a fixed-bed down-flow quartz reactor (i.d.=10 mm) connected downstream to a gas chromatograph fitted with a thermal conductivity detector. Prior to reactions, the catalysts were activated by reduction with H₂ (30 mL.min⁻¹) at 650 °C for 1 h. Next, the sample was brought to the reaction temperature (750 °C) under a pure N₂ flow. The reaction temperature was measured and controlled by a thermocouple inserted into the top of the catalyst bed.

The catalysts were tested under two conditions:

a) Oxidative reforming of methane (or oxidative reforming of model biogas): the feed was a mixture of the model biogas (60% of CH₄ and 40% of CO₂) and synthetic air (O₂: 21%, N₂: 79%) reaching a molar ratio of 1.5CH₄:1CO₂:0.25O₂; giving a total flow of 107 mL.min⁻¹ inside the reactor. Here, the conversions of CH₄ and CO₂ were calculated as:

$$R \ conversion \ (\%) = (R \ in - R \ out)/(R \ in) \qquad (4)$$

where R is the molar flow rate (mol. min⁻¹) of CH₄ or CO₂.

The selectivity was calculated as:

$$Selectivity \ to \ i = \frac{i_{produced}}{\left(\begin{array}{c} Molar \ flow \ rate \ of \\ CH_{4 \ converted} + CO_{2 \ converted} \end{array} \right)} \qquad (5)$$

where "i" is the molar flow rate (mol. min^{-1}) of product (H_2 or CO).

b) Partial oxidation of methane: the feed gases were in the molar proportion $2CH_4{:}1O_2$, stoichiometric for the POM, flowing at 107 mL.h^{-1}. The oxygen was added in the form of synthetic air (79% N_2, 21% O_2). Here, the CH_4 conversion was calculated as:

$$R\,conversion\,(\%) = (R\,in - R\,out)/(R\,in) \qquad (6)$$

where R is the molar flow rate (mol. min^{-1}) of CH_4.

The selectivity was calculated as:

$$Selectivity\,to\,i = \frac{i_{produced}}{\left(molar\ flow\ rate\ of\ CH_{4converted}\right)} \quad (7)$$

where "i" is the molar flow rate (mol. min^{-1}) of product (H_2 or CO or CO_2).

All reactions were carried out at 750 °C. Unconverted reactants and the reaction products were analyzed in-line by a gas chromatograph (GC, Varian 3800) equipped with two thermal conductivity detectors (TCD) and an automated injection valve. The products at the reactor outlet were divided into two streams, which were analyzed differently to obtain an accurate and complete analysis of the reaction products. In one stream, hydrogen and methane were separated in a 13X molecular sieve packed column, with nitrogen as carrier gas. In the other, N_2, CO_2, CH_4 and CO were separated in a Porapak-N packed column, with helium as carrier. Separated gases were monitored at each outlet with a TCD.

Carbon deposition rates were measured by Thermogravimetric analysis (from room temperature to 1000 °C) of the spent catalysts, in the presence of synthetic air.

RESULTS AND DISCUSSION

Characterization

Figure 1 shows the H_2-TPR profile of the catalysts. The major reduction peak is a result of NiO reduction; the PrZr supports did not show any relevant reduction peaks. According to the profiles shown in Figure 1, the NiO reduction peak increased as nickel content increased in the mixture. For the catalysts containing the three oxides ($NiO/ZrO_2/PrO_2$) it is clear that the maxima of each peak shifted downward as the nickel concentration increased in the mixture, meaning that NiO interacted stronger with the support at low nickel concentration in the mix-

ture. Probably at low nickel concentration, NiO species are more dispersed in the mixture and consequently more difficult to be reduced; this will be confirmed further by XRD analysis.

For comparison purposes, the TPR analysis of the 15NiZr catalyst (without Pr) was carried out. Comparing the profile of samples 15NiZr and 15NiPrZr, it can be seen that the addition of Pr to the mixture displaced the principal NiO reduction peak to lower temperatures. This last observation means that Pr promotes the reduction of NiO species, by weakening the Ni-O or H-H bonds.
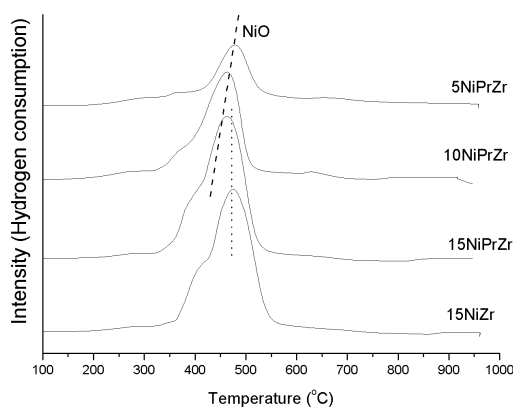

Figure 1: Temperature Programmed Reduction (H_2-TPR) profiles of the catalysts.

Table 1 shows the results of XRD, EDX and BET characterizations. The EDX results shown in Table 1 exhibit the elemental composition of nickel and praseodymium for each catalyst, these values are very close to the theoretical values. The catalyst surface area values and those of the support are low; there was no definite trend observed.

Table 1: Results for characterization by *in situ* XRD under reduction conditions (crystallite size of Niº), Adsorption-Desorption of N_2 (Surface area), EDX (elemental % for Ni and Pr in all catalysts) and metal dispersion (D_M).

Sample	Niº, nm (XRD)	t-ZrO_2, nm (XRD)	Surface area (m^2.g^{-1})	% Ni (wt; EDX)	% Pr (wt, EDX)	D_M (Niº)
PrZr	-	18.0	12		1.2	-
5NiPrZr	-	18.3	9	5.3	1.0	-
10NiPrZr	17	18.7	14	11.4	1.4	5.9
15NiPrZr	20	18.3	13	20.1	1.1	5.1
15NiZr	23	18.3	17	20.1	-	4.4

Figures 2(a) and 2(b) show the XRD patterns of the catalysts under room conditions and after reduction with H_2 at 650 °C. In Figure 2(a) it is clearly

seen that 1% of PrO$_2$ does not completely stabilize the tetragonal ZrO$_2$, as the mixture of the catalysts shows a mixture of monoclinic and tetragonal ZrO$_2$. The peaks related to the cubic NiO phase are observed in samples containing a nickel load above 10% wt; the sample with 5% wt of Ni (5NiPrZr) does not show any peak related to this phase, indicating that in this sample NiO particles do not form any large crystalline structure or they are undetectable by XRD analysis. In the XRD patterns of the samples (for both room condition and reduction condition) 10NiPrZr, 15NiPrZr and 15NiZr, it can be seen that the higher the nickel concentration in the mixture, the more intense the NiO (or Ni°) peaks.
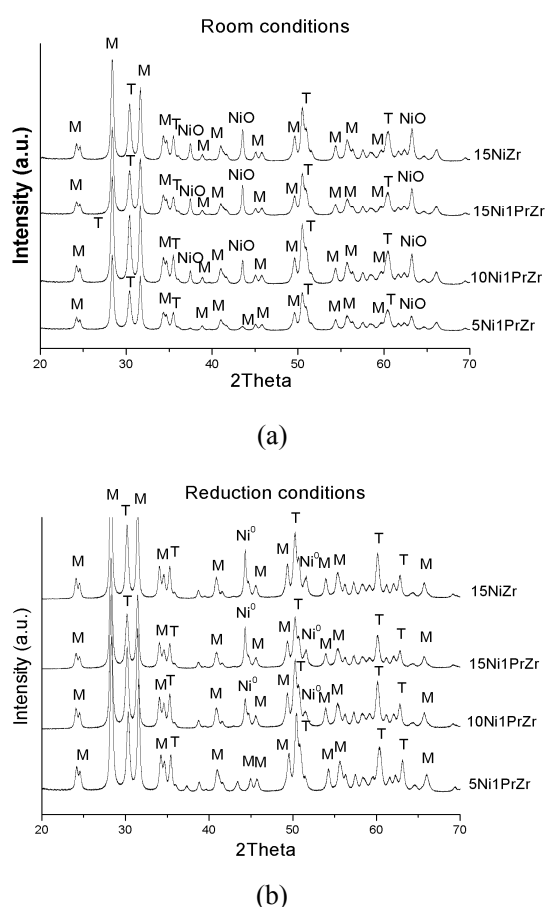

(a)

(b)

Figure 2: (a) X-Ray diffraction patterns (XRD) of catalysts under room conditions: Monoclinic ZrO$_2$ (M: JCPDS 13-307); Tetragonal ZrO$_2$ (T: JCPDS 14-534) and Cubic NiO (NiO: JCPDS 78-0643). (b) *in situ* X-Ray diffraction patterns (XRD) of catalysts under reduction conditions at 650 °C in H$_2$: Monoclinic ZrO$_2$ (M: JCPDS 13-307); Tetragonal ZrO$_2$ (T: JCPDS 14-534) and Cubic Ni° (Ni°: JCPDS 04-0850).

The crystallite size was calculated by the Scherrer equation (Chien and Chiang, 1990). These values indicate that the average crystallite size for ZrO$_2$ was not influenced by the increase in nickel content in the catalysts (as it did not vary among the catalysts). The average crystallite size of Ni° for 5NiPrZr was not possible to calculate, because no crystalline phase was detected by XRD analyses. As expected, the nickel content increased the average crystallite of Ni°, in 10NiPrZr (17 nm) and 15NiPrZr (20 nm). Comparing the average crystallite of Ni° for the promoted (15NiPrZr) and un-promoted sample (15NiZr, 23 nm) it is clearly seen that the addition of PrO$_2$ to the NiO/ZrO$_2$ mixture promoted the diminution of the Ni° crystallite size; this favors the metallic dispersion of nickel in the catalysts.

Some authors (Chien and Chiang, 1990; Bartholomew and Pannell, 1980; Jones and Bartohololomew, 1988; Zhang *et al*. 2008) have used the equation D$_M$ = 101/(*d*) satisfactorily to estimate the metal dispersion (D$_M$) of the active phase of the catalysts. That equation is valid for a population of spheroidal particles of the metal phase; (*d*) is the average crystallite size of Ni° (nm), and the constant was calculated on the basis of an assumed spherical particle and the density of nickel atoms on a polycrystalline Ni surface (1.54x10^{19} atom Ni.m^{-2}). According to Fagherazzi *et al*. (1995), Xu *et al*. (2005), and Venezia *et al*. (2003), the estimates calculated from that equation agree well with the metal dispersion values obtained by chemisorption techniques (chemisorption of H$_2$ or CO).
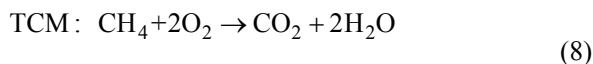
The D$_M$ values estimated in the present work are given in Table 1. According to these values, 10NiPrZr and 15NiPrZr catalysts showed high metal dispersion, despite 15NiZr and 15NiPrZr having the same nickel concentration, 15NiPrZr had higher metallic dispersion, owing to the presence of the PrO$_2$. This effect influenced the catalytic performance of the catalysts, as will be discussed in the catalytic test section.
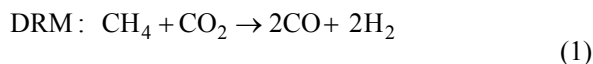
Catalytic Test

Partial Oxidation of Methane Reaction

The partial oxidation of methane can follow two types of mechanisms: the direct and the indirect mechanism. In the case of the indirect mechanism, also called the combustion-reforming mechanism, the reaction is carried out by the total combustion of methane reaction (TCM; Reaction 8), followed by dry reforming (DRM; Reaction 1) and steam reform-
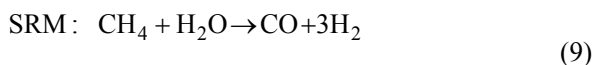
ing of methane (SRM; Reaction 9), to produce Syngas (H_2/CO):

$$TCM: CH_4 + 2O_2 \rightarrow CO_2 + 2H_2O \tag{8}$$

$$\Delta H° = -890 \text{ kJ.mol}^{-1}$$

$$DRM: CH_4 + CO_2 \rightarrow 2CO + 2H_2 \tag{1}$$

$$\Delta H° = 260.5 \text{ kJ.mol}^{-1}$$

$$SRM: CH_4 + H_2O \rightarrow CO + 3H_2 \tag{9}$$

$$\Delta H° = 225.4 \text{ kJ.mol}^{-1}$$

The global sum of reactions (TCM)+(DRM)+ 2x(SRM) is the POM reaction (Reaction 2), with a H_2/CO ratio of 2. The direct mechanism is the pyrolysis mechanism, in which the reactant products are transformed directly to H_2 and CO:

$$POM: CH_4 + 1/2O_2 \rightarrow CO + 2H_2 \tag{2}$$
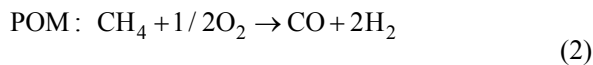
$$\Delta H° = -22.6 \text{ kJ.mol}^{-1}$$

The results of the catalytic test for the POM reaction are shown in Figure 3. According to these results, H_2, CO, CO_2 and traces of H_2O were found in the reaction product during each catalytic test, indicating that the combustion-reforming mechanism occurred on these catalysts.

As shown in Figure 3, the methane reactant conversions increased with Ni content, rising up to 15% (5NiPrZr<10NiPrZr<15NiZr<15NiPrZr). This trend was expected, as the high nickel concentration may produce more active Ni° sites; additionally, 15NiPrZr recorded the highest metallic dispersion (see Table 1). This means that the active Ni centers and oxygen

vacancies of the support (ZrO_2 and PrO_2) are in good proportion in the 15NiPrZ catalyst; these centers favored the conversion of CH_4 and O_2 into H_2 and CO, as principal products. Despite 15NiZr and 15NiPrZr having almost the same nickel concentration, 15NiPrZr performed better in the catalysis. This can be attributed to the higher metallic dispersion in comparison to 15NiZr, and also to the presence of PrO_2, which can also contribute to the catalysis due to its oxygen-vacancy properties (as will be discussed in further paragraphs).

The 5NiPrZr catalysts gave the worst performance in the POM, which may be related to their low nickel content. As seen in the characterization results, the low nickel content in 5NiPrZr formed very few NiO species available for reduction (see TPR profiles, Figure 1) and non-detectable crystalline arrangement of Ni° was found in the XRD patterns (see Figure 2); therefore, there were not many nickel active sites available for the catalysis.

The selectivity results for CO_2 and H_2/CO molar ratio are shown in Figure 3. The selectivities for H_2 and CO were close to the stoichiometric value for the best catalyst (close to 2 and 1 for H_2 and CO, respectively, for 15NiPrZr). In general for all catalysts, the selectivity followed a trend similar to that of CH_4 conversion, in which 5NiPrZr and 10NiPrZr showed the lowest H_2 and CO selectivity.

As expected, the PrZr support catalyzes the Total Combustion of Methane (TCM, Reaction 4) under the reaction conditions studied in this work, which is reasonable since it is known that this reaction is catalyzed by metal oxides (Choque *et al.*, 2010). This can explain the noticeable activity of the PrZr support in the methane conversion (almost 20% of CH_4 of the inlet-feed; Figure 3) under the reaction conditions studied.
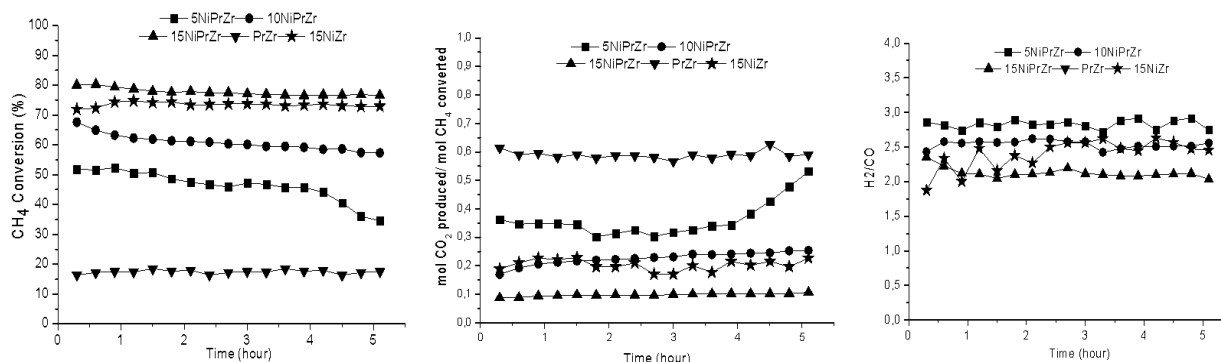

Figure 3: Results for the POM reactions over the catalysts at 700 °C, 1 atm for 5 hours of reaction time: CH_4 conversion: %, Selectivity: Mol CO_2 produced / Mol CH_4 converted.

On the other hand, the presence of nickel metal in the catalysts catalyzes the Dry Reforming and Steam Reforming of methane (by breaking the methane molecule C-H bond), leading to a POM reaction with the production of H_2 and CO and, consequently, to a dramatic diminution of the CO_2 selectivity profile, as seen in Figure 3.

All the catalysts have a noticeable CO_2 selectivity, maybe due to the presence of ZrO_2 and PrO_2, which are oxides and can catalyze TCM, thus producing CO_2. The good dispersion reached by 15NiPrZr with very low CO_2 selectivity (when compared to the others) may be due to the good distribution of Ni° active sites caused by the presence of the promoter PrO_2, in good equilibrium, as shown in the metallic dispersion results (Table 1). The 15NiPrZr catalyst performed better in the POM catalysis than the 15NiZr catalyst, which can be due to the presence of the promoter PrO_2, allowing the diminution of Ni° crystallite size (see Table 1) which favors a better dispersion of the metallic nickel in the catalyst, and also favors the catalysis of POM owing to the oxygen-vacancies present in the structure.

The H_2/CO molar ratio in Figure 3 shows that the 15NiPrZr sample had a H_2/CO molar ratio close to the stoichiometric value. In the other catalysts, such as 5NiPrZr, the H_2/CO ratio was higher than the stoichiometric value owing to the low selectivity to CO and high selectivity to CO_2, which increased this ratio. Furthermore, the presence of CO_2 and H_2 as the reaction product may favor the reverse water-gas shift reaction (RWGSR, Reaction 10) as well, as it is known that this reaction is favored at high temperature:
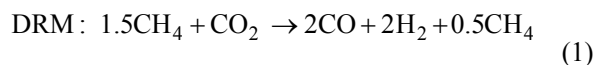
$$RWGSR : CO_2 + H_2 \leftrightarrow CO + H_2O$$

$$\Delta H° = 34.3 \text{ kJ.mol}^{-1}$$

(10)
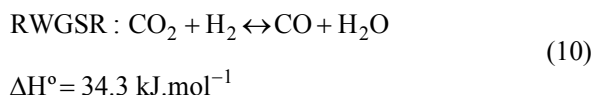
The occurrence of the RWGSR and the occurrence of TCM as the initial step in the POM may explain why the H_2/CO ratio does not reach the stoichiometric value. Despite liquid water being found in trace amounts, the quantity of the collected liquid followed the trend: PrZr (22 mmol.H_2O. min⁻¹) >5NiPrZr (12 mmol.H_2O. min⁻¹) >10NiPrZr (7 mmol.H_2O. min⁻¹) >15NiPrZr≈15NiZr (4 mmol.H_2O. min⁻¹); this tendency fits well with the selectivity to CO_2. Among all the catalysts studied, the samples 15NiPrZr and 10NiPrZr have the best H_2/CO molar ratio (close to 2).
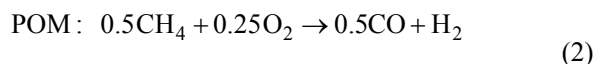
Oxidative Reforming of Methane Reactions

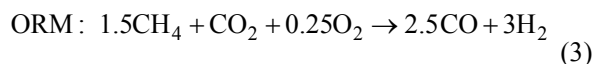In the oxidative reforming of methane, the molar ratio of methane and carbon dioxide is 1.5:1, which is favorable for the dry reforming of methane (DRM, Reaction 1) in the excess of methane, which is a typical composition of the major components in biogas:

$$DRM : 1.5CH_4 + CO_2 \rightarrow 2CO + 2H_2 + 0.5CH_4$$

$$\Delta H° = 260.5 \text{ kJ.mol}^{-1}$$

(1)

$$POM : 0.5CH_4 + 0.25O_2 \rightarrow 0.5CO + H_2$$

$$\Delta H° = -22.6 \text{ kJ.mol}^{-1}$$

(2)

$$ORM : 1.5CH_4 + CO_2 + 0.25O_2 \rightarrow 2.5CO + 3H_2$$

$$\Delta H° = 249.2 \text{ kJ.mol}^{-1}$$

(3)

Subsequently, the addition of oxygen to the inlet stream may help to increase the methane conversion, as it can react with the excess methane in the inlet stream by the partial oxidation of methane (POM, Reaction 2); both of these reactions lead to the Oxidative-reforming of methane (ORM, Reaction 3). During the DRM reaction, the reverse water-gas shift reaction (RWGSR, Reaction 6) can be favored.

As shown in Figure 4, similarly to that found in the POM reaction, the reactant conversions increased with increasing Ni content up to 15%. This increase is consistent with the high concentrations of nickel in the catalysts, which form more Ni° active sites; additionally, this is in strong relation to the high metallic dispersion found in 10NiPrZr and 15NiPrZr combined with the presence of the promoter PrO_2. This means that a good distribution of active Ni centers and oxygen vacancies in the support and promoter (ZrO_2 and PrO_2) in the catalyst 15NiPrZr (the best catalyst) favored the conversion of CH_4, CO_2 and O_2 into H_2 and CO under the reaction conditions.
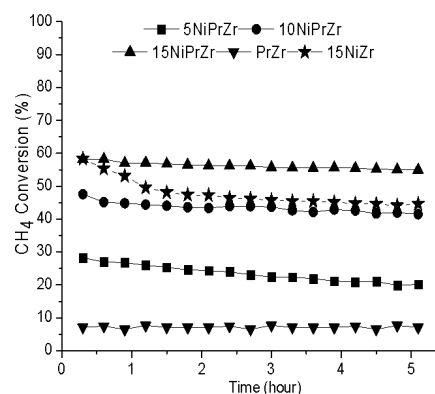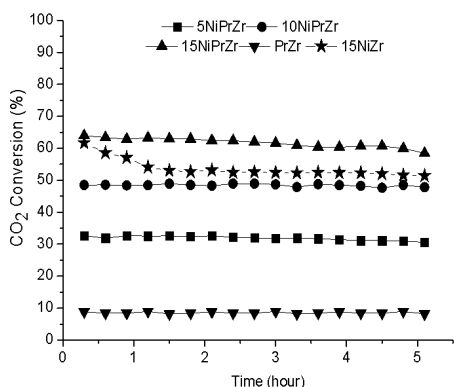
Figure 4: Results for the ORM reaction over the catalysts at 700 ºC, 1 atm for 5 hours of reaction time: CH_4 conversion and CO_2 conversion.

In all samples, the reactant conversion profile presented a slight fall during the 5 hours of reaction. This fall was most noticeable in the 5NiPrZr sample, owing to the very low nickel content, which led to low conversion values, resulting in poor stability. As revealed by *in situ* XRD, the sample 5NiPrZr had no detectable Niº crystallites under reduction conditions (see Table 1), which probably did not favor the formation of enough active sites for the breakdown of the C-H bonds of CH_4 molecules. Moreover, TPR analysis showed that this catalyst had only a few NiO species when compared to the other catalysts.

The catalytic activity of 15NiPrZr remained almost constant for 5 h, showing good stability (see Figure 4). The conversion of reactants on the support (PrO_2-ZrO_2) was very low (close to 8% for methane conversion) and, in the reaction without catalyst, was negligible under the reaction conditions studied. The promoted catalyst (15NiPrZr) performed better in the catalysis than the unpromoted catalyst (15NiZr). This can be explained by the fact that the addition of the promoter (PrO_2) reduced the Niº crystallite size in 15NiPrZr, as shown in Table 1, indicating that the promoter favored the metallic dispersion of Niº which favors the formation of more active centers. Additionally, as mentioned before, the mixture of PrO_2-ZrO_2 can catalyze the POM reaction (which in this case takes part in the ORM)

After the catalytic tests, traces of water were produced in all reactions, showing the occurrence of the reverse water-gas shift reaction (WGSR): $CO_2 + H_2 \leftrightarrow CO + H_2O$. This reaction may explain why the conversion of CO_2 is generally higher than that of CH_4. The H_2/CO ratio values are always lower than 1.2, which is the stoichiometric ratio. The low H_2/CO

ratio values for 15NiPrZr and 15NiZr were the best overall and closest to the stoichiometric value.

The conversion values of methane in the ORM were lower than conversion in the POM reaction, as expected, since the POM reaction is a faster reaction and highly favored by the presence of oxygen conductor-materials such as PrO_2 and ZrO_2, as in this case.

Coke Characterization

The images obtained by SEM analysis (in a carbon-rich region) of the catalysts after the partial oxidation of methane (the reaction where the catalysts performed better) are shown in Figure 5(a)-(b). The images correspond to the promoted sample (15NiPrZr, the best catalyst) and unpromoted sample (15NiZr), respectively. These images show the presence of filamentous carbon on the surface of the catalysts. Although these catalysts have almost equal nickel content, the presence of the promoter significantly modified the morphology of the carbon: very long and entangled filaments (and sparsely populated) were formed in sample 15NiPrZr, whereas the 15NiZr sample formed densely populated long filaments.
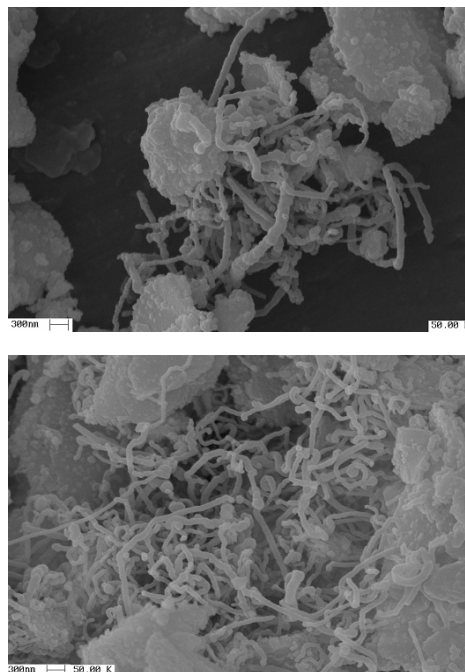

Figure 5: SEM images (x 50.000) of the catalysts after the POM reaction: (a) 15NiPrZr, (b) 15NiZr.

The TG profiles of the catalysts after the POM reaction are shown in Figure 6. The profiles of the catalysts containing the $NiO/PrO_2/ZrO_2$ mixture showed a very low general weight loss, indicating their low

coke deposition rate, in the case of 15NiPrZr this may have enabled their high catalytic performance. The 5NiPrZr and 10NiPrZr samples, which had the poorest catalytic performance in the POM, showed the lowest weight loss, which is reasonable since relatively low methane conversion values were reached (and consequently less carbon deposited). Although sample 15NiZr achieving good catalytic performance, this sample reached the highest weight loss, which indicates that the absence of PrO_2 in the mixture strongly affected the carbon deposition rates. At this point, it is possible to affirm that the promoter PrO_2 has two effects: to promote the metallic dispersion of Ni^o and to assist in coke removal due to the oxygen vacancies and oxygen mobility. Additionally, the 15NiZr sample had the largest Ni^o crystallite size, which can also explain the high carbon deposition rate (expressed as a high weight loss).
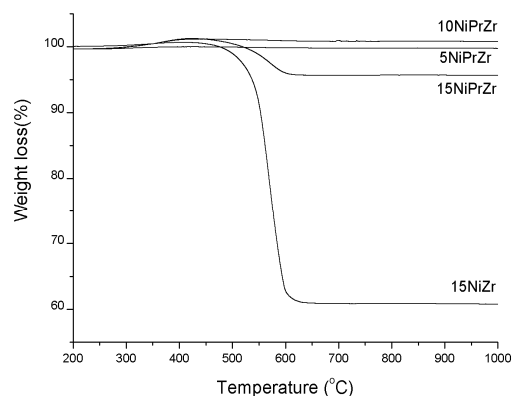

Figure 6: Thermogravimetric (TG) analyses of the catalysts, after the POM reaction (6 hours).

CONCLUSIONS

In the catalysis of the Oxidative-reforming of methane and Partial oxidation of methane, the conversion of reactants over the catalysts increased as the catalyst Ni content increased. The catalyst containing the mixture of the three oxides: $NiO/PrO_2/ZrO_2$ with 15 wt% of nickel (15NiPrZr catalyst) showed the best activity for the conversion of the reactants into Syngas with high selectivity for H_2 and CO.

The results of the present study suggest that the promoter PrO_2 has two roles: to promote the metallic dispersion of Ni^o and to assist in coke removal due to the oxygen vacancies and oxygen mobility. Despite a low concentration of nickel on the surface leading to metallic dispersion, very low nickel concentrations do not favor the methane transformation into Syngas.

The promoted catalyst (15NiPrZr) performed better in the catalysis than the unpromoted catalyst (15NiZr). This was explained by the fact that the addition of the promoter (PrO_2) reduced the crystallite size of Ni^o in 15NiPrZr favoring the metallic dispersion of Ni^o, which favors the formation of more active centers. Additionally, the mixture of PrO_2-ZrO_2 has catalytic activity in the POM reaction. The addition of PrO_2 to the $NiO/PrO_2/ZrO_2$ mixture modified the morphology of the carbon deposits.

ACKNOWLEDGEMENTS

REFERENCES

Asencios, Y. J. O., Nascente, P. A. P., Assaf, E. M., Partial oxidation of methane on NiO-MgO-ZrO₂ catalysts. Fuel, 97, 630 (2012a).

Asencios, Y. J. O., Assaf, E. M., Combination of dry reforming and partial oxidation of methane on NiO–MgO–ZrO₂ catalyst: Effect of nickel content. Fuel Proc. Technol., 106, 247 (2012b).

Asencios, Y. J. O., Bellido, J. D. A., Assaf, E. M., Synthesis of NiO–MgO–ZrO₂ catalysts and their performance in reforming of model biogas. Appl. Catal., A, 397, 138 (2011).

Asencios, Y. J. O., Rodella, C. B., Assaf, E. M., Oxidative reforming of model biogas over NiO–Y₂O₃–ZrO₂ catalysts. Appl. Catal. B, 132, 1 (2013).

Barroso, M. N., Galetti, A. E., Abello, M. C., Ni catalysts supported over MgAl₂O₄ modified with Pr for hydrogen production from ethanol steam reforming. Appl. Catal., A, 394, 124 (2011).

Bartholomew, C. H., Pannell, R. B., The stoichiometry of hydrogen and carbon monoxide chemisorption on alumina- and silica-supported nickel. J. Catal., 65, 390 (1980).

Burnham, A., Han, J., Clark, C. E., Wang, M., Dunn, J. B., Palou-Rivera, I., Life-cycle greenhouse gas emissions of shale gas, natural gas, coal, and petroleum. Environ. Sci. Technol., 46, 619 (2012).

Chien, S., Chiang, W. L., Catalytic properties of NiX zeolites in the presence of ceriumadditives. Appl. Catal., 61, 45 (1990).

Cheng, K., Virginie, M., Ordomsky, V. V., Cordier, C., Chernavskii, P. A., Ivantsov, M. I., Paul, S., Wang, Y., Khodakov, A. Y., Pore size effects in

high-temperature Fischer–Tropsch synthesis over supported iron catalysts. J. Catal., 328, 139 (2015).

Choque, V., Ramirez de la Piscina, P., Molyneux, D., Homs, N., Ruthenium supported on new TiO_2–ZrO_2 systems as catalysts for the partial oxidation of methane. Catal. Today, 149, 248 (2010).

Couto, N., Rouboa, A., Silva, V., Monteiro, E., Bouziane, K., Influence of the biomass gasification processes on the final composition of syngas. Energy Procedia, 36, 596 (2013).

Fagherazzi, G., Benedetti, A., Polizzi, S., Di Mario, A., Pinna, F., Structural investigation on the stoichiometry of β-PdH_x in Pd/SiO_2 catalysts as a function of metal dispersion. Catal. Lett., 32, 293 (1995).

Gallego, G. S., Marına, J. G., Batiot-Dupeyrat, C., Barrault, J., Mondragon, F., Influence of Pr and Ce in dry methane reforming catalysts produced from La1_xAxNiO3_d perovskites. Appl. Catal., A, 369, 97 (2009).

Gamba, O., Moreno, S., Molina, R., Catalytic performance of Ni-Pr supported on delaminated clay in the dry reforming of methane. Int. Journal of Hydrogen Energ., 36, 1540 (2011).

Jones, R. D., Bartholomew, C. H., Improved flow technique for measurement of hydrogen chemisorption on metal catalysts. Appl. Catal., A, 39, 77 (1988).

Liu, C. J., Ye, J., Jiang, J., Pan, Y., Progresses in the preparation of coke resistant Ni-based catalyst for steam and CO_2 reforming of methane. ChemCatChem., 3, 529 (2011).

Lucrédio, A. F., Assaf, E. M., Reforming of a model biogas on Ni and Rh Ni catalysts: Effect of adding La. Fuel Proc. Technol., 102, 124 (2012).

Marcos, P. J. B., Gouvêa, D., Effect of MgO segregation and solubilization on the morphology of ZrO_2 powders during synthesis by the Pechini method. Cerâmica, 50, 38 (2004).

Mudd, G. M., Global trends and environmental issues in nickel mining: Sulfides versus laterites. Ore Geology Reviews, 38, 9 (2010).

Olah, G. A., Goeppert, A., Czaun, M., Surya, G. K., Bi-reforming of methane from any source with steam and carbon dioxide exclusively to metgas (CO–$2H_2$) for methanol and hydrocarbon synthesis. J. Am. Chem. Soc., 1351, 648 (2013).

Ramos, A. L. D., Marques, J. J., Santos, V., Freitas, L. S., Melo Santos, R. G. V., Souza, M. V. M., Atual estágio de desenvolvimento da tecnologia GTL e perspectivas para o Brasil. Quím. Nova, 34, 1704 (2011). (In Portuguese).

Rueangjitt, N., Akarawitoo, C., Chavadej, S., Production of hydrogen-rich syngas from biogas reforming with partial oxidation using a multistage AC gliding arc system, plasma. Chem. Plasma Process, 32, 583 (2012).

Sun, D., Li, X., Ji, S., Cao, L., Effect of O_2 and H_2O on the tri-reforming of the simulated biogas to syngas over Ni-based SBA-15 catalysts. J. Nat. Gas Chem., 19, 369 (2010).

Turn, C., Kinoshita, Z., Zhang, D., Ishimura, J., An experimental investigation of hydrogen production from biomass gasification. International Journal of Hydrogen Energy, 23, 641 (1998).

Venezia, A. M., Liotta, L. F., Pantaleo, G., La Parola, V., Deganello, G., Beck, A., Koppány, Z., Frey, K., Activity of SiO_2 supported gold-palladium catalysts in CO oxidation. App. Catal., A, 251, 359 (2003).

Wright, M. C., Court, R. W., Kafantaris, F. C. A., Spathopoulos, F., Sephton, M. A., A new rapid method for shale oil and shale gas assessment. Fuel, 153 231-239 (2015).

Xu, D., Li, W., Duan, H., Ge, Q., Xu, H., Reaction performance and characterization of Co/Al_2O_3 Fischer–Tropsch catalysts promoted with Pt, Pd and Ru. Catal. Lett., 102, 229 (2005).

Zhang, J., Wang, H., Dalai, A., Effects of metal content on activity and stability of Ni-Co bimetallic catalysts for CO_2 reforming of CH_4. App. Catal., A, 339, 121 (2008).